# The Intrinsic Protein Flexibility of Endogenous Protease Inhibitor TIMP-1 Controls Its Binding Interface and Affects Its Function

**ARTICLE** *in* BIOCHEMISTRY · JULY 2010

Impact Factor: 3.02 · DOI: 10.1021/bi902141x · Source: PubMed



**7 AUTHORS**, INCLUDING:

Dmitry Tworowski
Weizmann Institute of Science
**13** PUBLICATIONS **247** CITATIONS
SEE PROFILE

Orly Dym
Weizmann Institute of Science
**46** PUBLICATIONS **2,696** CITATIONS
SEE PROFILE

Irit Sagi
Weizmann Institute of Science
**59** PUBLICATIONS **1,348** CITATIONS
SEE PROFILE

6184 *Biochemistry* **2010,** *49,* 6184–6192
DOI: 10.1021/bi902141x

BIOCHEMISTRY
including biophysical chemistry & molecular biology
*Article*

# The Intrinsic Protein Flexibility of Endogenous Protease Inhibitor TIMP-1 Controls Its Binding Interface and Affects Its Function[†]

Moran Grossman,[‡] Dmitry Tworowski,[‡] Orly Dym,[‡] Meng-Huee Lee,[§] Yaakov Levy,[‡] Gillian Murphy,[§] and Irit Sagi*[,‡]

[‡]*Department of Structural Biology, Weizmann Institute of Science, Rehovot, Israel, and* [§]*Department of Oncology, Cambridge University, Cancer Research UK Cambridge Research Institute, Li Ka Shing Centre, Cambridge CB2 0RE, United Kingdom*

*Received December 14, 2009; Revised Manuscript Received June 13, 2010*

ABSTRACT: Protein flexibility is thought to play key roles in numerous biological processes, including antibody affinity maturation, signal transduction, and enzyme catalysis, yet only limited information is available regarding the molecular details linking protein dynamics with function. A single point mutation at the distal site of the endogenous tissue inhibitor of metalloproteinase 1 (TIMP-1) enables this clinical target protein to tightly bind and inhibit membrane type 1 matrix metalloproteinase (MT1-MMP) by increasing only the association constant. The high-resolution X-ray structure of this complex determined at 2 Å could not explain the mechanism of enhanced binding and pointed to a role for protein conformational dynamics. Molecular dynamics (MD) simulations reveal that the high-affinity TIMP-1 mutants exhibit significantly reduced binding interface flexibility and more stable hydrogen bond networks. This was accompanied by a redistribution of the ensemble of substrates to favorable binding conformations that fit the enzyme catalytic site. Apparently, the decrease in backbone flexibility led to a lower entropy cost upon formation of the complex. This work quantifies the effect of a single point mutation on the protein conformational dynamics and function of TIMP-1. Here we argue that controlling the intrinsic protein dynamics of MMP endogenous inhibitors may be utilized for rationalizing the design of selective novel protein inhibitors for this class of enzymes.

Accumulating reports highlight the importance of conformational dynamics to protein functions such as enzyme catalysis, signal transduction, allosteric transitions, inhibition, and ligand binding (*1*−*5*). Protein flexibility was also hypothesized to play a critical role in aspects of protein−protein molecular recognition, including drug−protein interactions (*6*). The intrinsic structural plasticity of proteins is manifested in the differences found in crystal and NMR[1] structures of bound and free protein ligands, mainly in the binding sites. In addition, analyses of site-directed mutagenesis of protein exosites were shown to affect protein function and stability (*7*). These findings have raised the notion that protein function and reactivity may be perturbed by a network of interactive residues within a protein moiety. For example, the rate of hydride transfer in dihydrofolate reductase (*8*), the resistance of flaviviruses to antibodies (*9*), the inhibition of serine protease by the serine protease inhibitor Eglin C (*10*), and the function of yeast histone acetyltransferase (*11*) are all dependent not only on active site residues but also on distal structural elements. Pan et al. demonstrated that such "molecular allosterism" may originate from a functional coupling between distal residues within the protein core that communicate by modulating the conformational ensemble (*12*). Thus, to appreciate the effect of small-scale perturbations on protein function, one should also consider the intrinsic conformational dynamics of the protein in question.

Here we used quantitative experimental and theoretical approaches to reveal the molecular interaction of the clinically important enzyme−endogenous inhibitor complex (MMP−TIMP). Here MMP−TIMP is used as a model system to elucidate the interplay between protein flexibility and function. The human MMP family comprises a large group of structurally homologous zinc-dependent endopeptidases that perform a wide variety of biological roles. Originally described as proteinases involved in extracellular matrix (ECM) catabolism, these enzymes were later found to play major roles as initiators of signaling pathways in many aspects of biology, ranging from cell proliferation, differentiation, and communication to pathological states associated with tumor metastasis, inflammation, tissue degeneration, and cell death (*13*−*17*). An important mechanism for the regulation of the activity of MMPs in vivo is formation of a tight, noncovalent 1:1 stoichiometric complex with a family of homologous TIMPs.

Currently, four TIMP variants that are 40−50% identical in sequence have been identified, namely TIMP-1−4. TIMPs, as revealed by the available crystal and NMR structures of MMP−TIMPs and free TIMPs, are folded into two distinct domains (*18*−*22*). The N-terminal domain is composed of a five-strand $\beta$-barrel, whereas the C-terminal domain is composed mainly of $\beta$-sheets and is structurally less defined. Extensive mutagenesis analysis has shown that the N-terminal domain of TIMP-1 (N-TIMP-1) can solely inhibit MMPs (*23*−*26*), though with a slightly reduced affinity. Figure 1 shows the structural model of the enzyme−inhibitor (MT1-MMP−N-TIMP-1) complex

[†]This work was supported by the Israel Science Foundation, by the Clotide and Mauricio Pontecorvo funds, and by a research grant from Mr. and Mrs. Michael Ambach to I.S. G.M. and M.-H.L. are supported by Cancer Research UK, Hutchison Whampoa, and the BBSRC, UK.

*To whom correspondence should be addressed: Department of Structural Biology, The Weizmann Institute of Science, Rehovot 76100, Israel. Telephone: 972 8 9342130. Fax: 972 9 9344154. E-mail: irit.sagi@weizmann.ac.il.

[1]Abbreviations: NMR, nuclear magnetic resonance; TIMP, tissue inhibitor of metalloproteinase; MMP, matrix metalloproteinase; MD, molecular dynamics; MT, membrane-type; WT, wild-type; rmsd, root-mean-square deviation.

 Published on Web 06/14/2010 

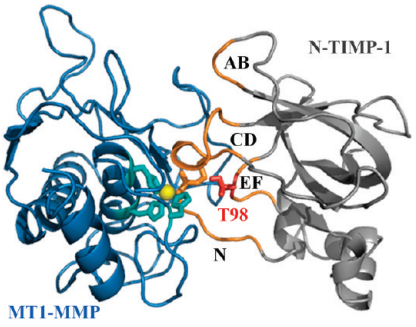


FIGURE 1: Formation of MT1-MMP:N-TIMP-1 complex. Model of binding of N-TIMP-1 to MT1-MMP derived from homology modeling. MT1-MMP is colored blue and TIMP gray. The catalytic conserved histidines of MMP and cysteine 1 of TIMP, which coordinate the $Zn^{2+}$ (yellow sphere), are shown as sticks. The TIMP binding interface (orange) is mainly composed of the N-terminal segment that approaches the active site, the AB loop ($Thr^{33}$−$Tyr^{35}$), the CD loop ($Ala^{65}$−$Cys^{70}$), and the EF loop ($Thr^{97}$−$Ser^{100}$). The pivotal residue, threonine 98 ($Thr^{98}$), is shown as red sticks.

generated by molecular homology modeling (see Materials and Methods for details). The N-TIMP binding interface (MMP binding ridge) is mainly composed of flexible regions such as the N-terminal segment ($Cys^{1}$−$Pro^{6}$, TIMP-1 numbering), which approaches the active site, and connector loops such as the peripheral AB loop ($Thr^{33}$−$Tyr^{35}$,), the CD loop ($Ala^{65}$−$Cys^{70}$), and the EF loop ($Thr^{97}$−$Ser^{100}$) (*18*).

Despite its structural and functional similarities to wild-type (WT) TIMP-2−4, WT TIMP-1 does not form a tight-binding complex with MT1-MMP (*27*, *28*). A single point mutation of threonine 98 ($Thr^{98}$), located in the EF loop, to leucine (T98L) transformed the N-terminal domain of TIMP-1 (N-TIMP-1) into a tight-binding inhibitor of MT1-MMP. This mutation retained the original inhibitory character of N-TIMP-1 toward other MMP family members. Remarkably, the mutated residue in N-TIMP-1 had not previously been noted as being pivotal for binding, since it is located at the periphery of the binding interface. Moreover, point mutations of isoleucine, methionine, and valine also resulted in high-affinity inhibitors, whereas mutations of serine, glycine, and alanine resulted in no inhibition. The molecular basis underlying the role of mutations in $Thr^{98}$ and the difference in the inhibitory profile remain elusive and cannot be understood with steric reasoning (*29*).

In this work, we quantify and rationalize the dramatic effect of single point mutations in the N-terminus of TIMP-1 on protein function. To characterize the properties of binding of the different N-TIMP-1 variants to MT1-MMP, we have assessed the interactions of MT1-MMP with the inhibitors by surface plasmon resonance (SPR) spectroscopy. These measurements indicate that the single point mutation affects only the association constant. Using MD simulations on a homology model of MT1-MMP in complex with N-TIMP-1 [generated from available Protein Data Bank (PDB) structures], we demonstrate that mutations in $Thr^{98}$ affect the overall intrinsic protein flexibility, especially of the binding interface. In addition, our data suggest that formation of the enzyme−inhibitor complex is thermodynamically more favorable for mutants exhibiting high-affinity versus low-affinity binding constants. Recently, we have determined the crystal structure of the complex formed between MT1-MMP (catalytic domain) and one of the high-affinity N-TIMP-1 mutant. This structure provides structural insights into the observed decrease in binding interface flexibility. Here we argue that control over protein flexibility of TIMP binding interfaces may be used to monitor their physiological protein−protein interactions. Thus, intrinsic protein flexibility provides an additional aspect of molecular regulation in these clinically important endogenous inhibitors.

## MATERIALS AND METHODS

*Materials*. All chemicals and reagents were purchased from Sigma unless otherwise stated. Restriction enzymes and Pfu polymerases for polymerase chain reaction (PCR) were obtained from New England Biolabs.

*Protein Expression and Purification*. The N-terminal domains of TIMP-1 and TIMP-2 were purified as described previously (*30*). The pRSET N-TIMP-1 T98L clone was generated using the guidelines described in the QuikChange site-directed mutagenesis kit (Stratagene), but using Phusion polymerase (Finnzyme) for DNA amplification. The catalytic domain of human MT1-MMP (residues 114−290) was cloned into the pET3a expression vector with a His tag at the N-terminus and was expressed in the *Escherichia coli* BL21 strain. Following expression, the enzyme was accumulated in the fraction of inclusion bodies. The *E. coli* cells were harvested, washed, lysed, and centrifuged to isolate the inclusion bodies. Then, they were suspended in 6 M urea and 50 mM Tris (pH 8.5) to solubilize the protein. The protein was purified on a Ni-NTA column, diluted to 50 $\mu$g/mL with 6 M urea, 50 mM Tris, and 150 mM $\beta$-mercaptoethanol (pH 8.5), and then refolded by slow dialysis against decreasing concentrations of urea. Finally, the enzyme was purified by gel filtration in 50 mM Tris (pH 7.5), 100 mM NaCl, and 5 mM $CaCl_2$ on a column of Superdex 75 (2.6 cm × 60 cm).

*Protein Assessment of Activity by Titration*. The concentration of active MT1-MMP was determined by titration with the hydroxamate inhibitor GM6001 ($K_i$ = 0.5 nM). The concentration and activity of active TIMPs were assessed and determined by titration against MT1-MMP as reported previously (*31*).

*Determination of Equilibrium Constants Using SPR*. SPR analysis was performed using a BIAcore 3000 instrument; experiments were performed at 298 K. The BIAcore system, sensor chip CM5, HBS [10 mM Hepes, 3.4 mM EDTA, 150 mM NaCl, and 0.05% surfactant P20 (pH 7.4)], and the amine coupling kit were obtained from Pharmacia Biosensor AB (Uppsala, Sweden). The amine coupling kit was used to activate the carboxymethylated dextran surface of the sensor chip. Immobilization was achieved via injection of MT1-MMP (50 $\mu$L, 10 $\mu$M in sodium acetate, 20 mM, pH 4.6, 20 $\mu$L/min). Residual NHS esters were inactivated with ethanolamine. Each binding experiment was performed with a constant flow of 10 $\mu$L/min, at 298 K. Prior to injection, the system was primed with MT1-MMP binding buffer [50 mM Tris (pH 7.5), 100 mM NaCl, and 5 mM $CaCl_2$]. Fifty microliters of analyte (N-TIMP-1, 0.8−10 $\mu$M; N-TIMP-1 T98L, 0.8−10 $\mu$M; and N-TIMP-2, 0.1−4 $\mu$M) was injected over the surface for the association phase. The surface was regenerated with 20 $\mu$L of NaOH (1 mM) followed by an extensive washing of the system and by equilibration of the surface with buffer. To estimate the increase in response units (RU) resulting from the nonspecific effect of protein on the bulk refractive index, we also measured binding of protein to a control surface with no immobilized ligand. This nonspecific signal was subtracted from the measured signal for the interaction between MT1-MMP and N-TIMPs at all the concentrations analyzed.

Association and dissociation rate constants were determined by analyzing the appropriate regions of the sensogram using BIAevaluation version 2.1 (Pharmacia).

*In Silico Modeling of TIMP Variants*. The initial coordinates of TIMP-1 were obtained from the PDB structures of TIMP-1 in complex with MMP-3 [PDB entry 1UEA (*18*)]. Similarly, the coordinates of MT1-MMP were obtained from the complex of TIMP-2 with MT1-MMP [PDB entry 1BUV (*21*)]. The initial homology model of the complex of TIMP-1 bound to MT1-MMP was prepared as follows. α-Carbon (Cα) atoms from identical residues of MMP-3 (chain A) and MT1-MMP (chain B) were used for structural alignment of the MMP-3−TIMP-1 complex with the MT1-MMP−TIMP-2 complex (the reference coordinates). Clashes between the TIMP-1 and MT1-MMP atoms were removed after 1000 steps of rigid-body minimization. To quantify the effect of only the N-terminal domain, the C-terminal domain of TIMP-1 (starting from residue 127) was deleted. The new complex between N-TIMP-1 and MT1-MMP was further refined by 1000 steps of steepest-descent energy minimization applied to all atoms. Minimization protocols were performed with the amber99 force field by using *minrigid* and *minimize* programs from TINKER version 4.2 (*32*). Mutations were introduced at position 98 of N-TIMP-1 protein using Chimera (*33*), and the optimal side chain rotamer was evaluated in the context of their structural environment. This initial model was used in our MD simulations prior to our protein crystallography analysis (see the text).

*Molecular Dynamics Simulations*. The MD simulations of WT N-TIMP-1 and its mutants were conducted using GROMACS version 3.3.1. The simulation protocol includes the following stages. (1) One thousand steepest descent minimization steps were conducted in vacuum (1000 steps) of the mutated residues only, while keeping other atoms restrained at their initial positions. (2) Minimized structures were placed at the center of a SPC water box (*34*, *35*). (3) The total charge of each system was neutralized by sodium or chloride ions. (4) The energy of the solvated structures was minimized by using the steepest descent method followed by conjugate gradient minimization. (5) To relax water molecules, a 100 ps MD simulation was performed at constant pressure and temperature $T$ (300 K). The positions of protein non-hydrogen atoms were restrained by a force constant of 1000 kJ mol$^{-1}$ Å$^{-1}$. (6) Trajectories (20 ns) were sampled at a constant volume ($V$) and temperature ($T$) using the Berendsen thermal bath (*36*). Three simulations were performed for each variant starting from different initial velocities. The configurational entropy of the inhibitor variants in the unbound form was estimated using Schlitter's method after the global translation and rotation of the molecule within the simulation box are removed by least-squares fitting to a reference structure, prior to the analysis (*37*).

*Preparation of the MT1-MMP−N-TIMP-1 Complex for Crystallization*. The N-TIMP-1 V4A/P6V/T98L high-affinity mutant was expressed and purified as described previously (*30*). Samples of MT1-MMP (1.53 mg, 76.6 nmol) and N-TIMP-1 V4A/P6V/T98L (3 mg, 200 nmol) were mixed and incubated overnight at room temperature with gentle stirring in 50 mM Tris (pH 7.5), 150 mM NaCl, and 5 mM $CaCl_2$. The MT1-MMP−N-TIMP-1 complex was separated from the remaining free N-TIMP-1 by gel filtration with a column of Superdex 75 (2.6 cm × 60 cm).

*Crystallization, Data Collection, and Refinement*. Crystals of the MT1-MMP−N-TIMP-1 complex were obtained by the hanging drop method. The crystals were grown from a solution of 100 mM Bis-Tris (pH 5.5) and 20% PEG 3350. Crystals formed in space group $P2_1$ with two complexes in the asymmetric unit cell with a $V_m$ of 2.37 Å$^3$/Da and the following cell constants: $a$ = 59.69 Å, $b$ = 63.65 Å, $c$ = 87.16 Å, and $\beta$ = 105.86°. The data to 2.05 Å resolution from a single crystal were collected on a Rigaku R-AXIS IV$^{++}$ imaging plate area detector mounted on a Rigaku RU-H3R generator with Cu Kα radiation focused by Osmic confocal mirrors. The diffraction data were indexed and integrated using HKL2000 (*38*). Integrated intensities were scaled using SCALEPACK (*38*). The structure factor amplitudes were calculated using TRUNCATE from the CCP4 program suite (*39*). The structure of the MT1-MMP−N-TIMP-1 complex was determined by molecular replacement using the known complex structure of the wild-type membrane type 1 MMP (MT1-MMP) and the tissue inhibitor of metalloproteinase 2 (TIMP-2) [PDB entry 1BQQ (*21*)] as a starting model. The refinement was conducted using CCP4/Refmac5 (*40*). The model was used to build the electron density maps ($2F_{obs} - F_{calc}$ and $F_{obs} - F_{calc}$) using COOT (*41*). Water molecules were built into peaks greater than 3$\sigma$ in the $F_{obs} - F_{calc}$ maps. Finally, the MT1-TIMP1 model was evaluated with MolProbity (*42*). Because of the lack of electron density, residues 50−56 of TIMP-1 could not be positioned unambiguously. Other residues that did not have electron density and therefore were modeled as glycine or alanine were those at positions 117, 118, 120, 123, 158, 169, and 281. The details of the refinement statistics of the MT1-TIMP1 structure are presented in Table 1 of the Supporting Information. The coordinates and structure factors for the MT1-TIMP1 structure have been deposited in the RCSB PDB as entry 3MA2.

Table 1: SPR Analysis of the Binding among WT N-TIMP-1, N-TIMP-1 T98L, and N-TIMP-2 and MT1-MMP Revealed That the T98L Single Point Mutation Affects the Kinetic Association Constant[a]

| | $k_a$ (M$^{-1}$ s$^{-1}$) | $k_d$ (s$^{-1}$) | $K_D$ (M) |
|---|---|---|---|
| N-TIMP-1 | $1.82 \times 10^3$ | $2.78 \times 10^{-3}$ | $1.53 \times 10^{-6}$ |
| N-TIMP-1 T98L | $3.35 \times 10^4$ | $2.91 \times 10^{-3}$ | $8.70 \times 10^{-8}$ |
| N-TIMP-2 | $3.58 \times 10^5$ | $2.01 \times 10^{-2}$ | $5.61 \times 10^{-8}$ |

[a]The kinetic dissociation binding constant ($K_D$) was obtained by dividing the kinetic dissociation rate constant ($k_d$) by the kinetic association rate constant ($k_a$).

## RESULTS AND DISCUSSION

To quantify the effect of the T98L mutation on N-TIMP-1, we determined the binding constants for MT1-MMP−N-TIMP interactions using real-time SPR analysis. To this end, diluted solutions of various concentrations of N-TIMPs were passed over immobilized MT1-MMP (catalytic domain) as a function of time. The data were fitted using a monophasic model for nonlinear curve fitting, taking into account possible mass transport. Kinetic association ($k_a$) and dissociation ($k_d$) rate constants were calculated using global spectrum analysis as well as by fitting the individual association and dissociation phases. The full data sets collected for each TIMP variant are shown in Figure S1 of the Supporting Information. SPR analysis (Table 1) revealed that WT N-TIMP-1 binds MT1-MMP with a $k_a$ of $1.8 \times 10^3$ M$^{-1}$ s$^{-1}$ and a $k_d$ of $2.73 \times 10^{-3}$ s$^{-1}$, whereas N-TIMP-2 binds MT1-MMP with a $k_a$ of $3.6 \times 10^5$ M$^{-1}$ s$^{-1}$ and a $k_d$ of $2.0 \times 10^{-2}$ s$^{-1}$. The kinetic dissociation binding constant ($K_D$) of WT N-TIMP-2 is 2 orders of magnitude smaller than that of WT N-TIMP-1, indicating the weak affinity between MT1-MMP and WT

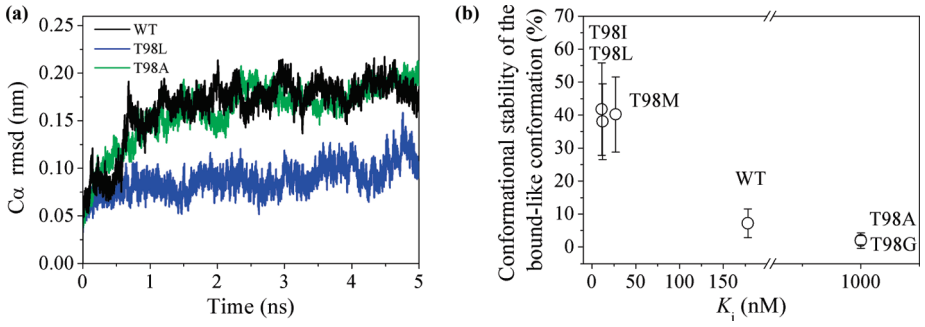


FIGURE 2: Interface flexibility of MMP-TIMP. (a) The rmsd of the interfacial Cα atoms of WT N-TIMP-1 (black), N-TIMP-1 T98L (blue), and N-TIMP-1 T98A (green) along the first 5 ns of the simulation. The curves were obtained after averaging several MD trajectories for each variant using Origin. The simulations show that the free T98L mutant of N-TIMP-1 is trapped in the bound conformation for a longer period of time than the wild type and the T98A mutant. These simulations of the free inhibitors support the notion that the T98L mutant favors the bound conformation with MT1-MMP even in its unbound state. Full trajectories are provided in the Supporting Information. (b) Correlation between inhibition constants ($K_i$) and the conformational stability of the bound-like state of N-TIMP variants. $K_i$ values were taken from ref *44*. The stability of the bound-like state was defined as the percentage of simulation time during which the N-TIMP-1 interface backbone remains close to its bound conformation (within 0.1 nm rmsd). High-affinity mutants (T98L, T98I, and T98M) populate more frequently the bound-like state than low-affinity mutants (WT, T98G, and T98A).

N-TIMP-1. The N-TIMP-1 T98L mutant regained high-affinity binding to MT1-MMP with a $k_a$ of $3.3 \times 10^4\ M^{-1}\ s^{-1}$ and a $k_d$ of $2.9 \times 10^{-3}\ s^{-1}$, resulting in a 2 order of magnitude decrease in $K_D$, similar to the case for N-TIMP-2, the in vivo inhibitor of MT1-MMP. The single point mutation, T98L, affected only the association constant of the inhibitor rather the dissociation constant, emphasizing the importance of this residue to the onset of the molecular recognition process between the two proteins (*43*), despite its location at the periphery of the binding interface. Thus, the enhanced binding affinity of the T98L mutant originates from a tighter enzyme−inhibitor complex, suggesting the formation of new interface interactions.

The previously reported molecular docking model of TIMP-1 in complex with a member of the MT-MMP family suggested that steric clashes between the C-terminal domain of TIMP-1 and the catalytic domain of MT3-MMP may hinder the formation of a tight-binding complex (*29*). However, this molecular model does not provide a plausible explanation for why the N-terminal domain of TIMP-1 fails to form such a complex with MT-MMPs in the absence of the proposed C-terminal steric clashes. Importantly, MMP-TIMP association is driven by both protein−protein and metal−protein interactions. Thus, TIMP should reside in a proper conformation that will enable it to directly bind the catalytic zinc ion and interact with the enzyme surface.

To this end we set to examine the effect of high- and low-affinity single point mutations at $Thr^{98}$ on the intrinsic protein flexibility of TIMP-1 and on its molecular conformations. We performed MD simulations with several variants of N-TIMP-1. The bound conformation of the WT inhibitor in this model (Figure 1), as well as of the in silico made mutants (T98L, T98A, T98G, T98I, and T98M), served as the initial structure for the MD simulations. To achieve sufficient time for equilibration, we conducted three 20 ns trajectories for each of the N-TIMP-1 variants, at 300 K, starting from different initial velocities (see Materials and Methods). Figure 2a shows time-dependent rmsd (root-mean-square deviation) profiles of the binding interface backbone atoms of N-TIMP-1 variants along the first 5 ns of the 20 ns MD simulations averaged over all trajectories (see Figure S2 of the Supporting Information for full trajectories). The rmsd values represent the deviation from an initial reference-bound-like conformation of TIMP derived from the enzyme−inhibitor homology modeling (Figure 1). During the simulations (and up to 5 ns), the interface backbone of the high-affinity T98L mutant possessed lower rmsd values than the low-affinity WT and the T98A mutant. This trend persisted in all the individual trajectories. A similar trend in interface dynamic behavior was observed for various high- and low-affinity inhibitory mutants (see Figure S3 of the Supporting Information). These results suggest that the high-affinity N-TIMP-1 mutants exhibit significantly reduced binding interface flexibility compared with the low-affinity mutants and WT. Thus, the high-affinity variants sample the bound-like conformation more significantly even in their unbound state. This is also apparent from the correlation between the experimental inhibition constants ($K_i$) of high- and low-affinity inhibitor mutants found by Lee et al. (*30*, *44*) and their conformational stability in a bound-like state (Figure 2b). The stability of this state was defined as the percentage of simulation time during which the backbone of the N-TIMP-1 binding interface remains close to its bound conformation (within 0.1 nm rmsd). Figure 2b demonstrates that the high-affinity N-TIMP-1 mutants populate the bound-like state more significantly than their analogous low-affinity mutants. To evaluate the conformational dynamics of the N-TIMP-1 variants, we calculated the average distance between the α-carbons of each residue pair, $\langle R_{ij} \rangle$. Figure 3 shows pairwise two-dimensional maps of internal distances describing the dynamics of the N-TIMP-1 protein binding interface in the unbound state. WT N-TIMP-1 (Figure 3a) and the low-affinity mutant T98A (Figure 3b) have a very flexible interface compared with the high-affinity mutant, T98L (Figure 3c), which possesses reduced flexibility or more confined conformational dynamics. The difference in flexibility is also reflected by superposition of seven snapshots (taken every 1 ns along the last 7 ns of simulation) of all structures.

The variance in binding interface flexibility is expected to affect the binding entropy of the various MMP-TIMPs. The conformational entropies were estimated from the MD trajectories for all N-TIMP-1 variants in the unbound state using Schlitter's approximation (*37*, *45*). Figure 4a shows a clear trend between $K_i$ values and the conformational entropy of the unbound state ($S_{unbound}$) of the different N-TIMP-1 variants. WT and low-affinity N-TIMP-1 mutants exhibit high conformational entropy compared with that of high-affinity mutants (in their free state). The reduced conformational entropy of the high-affinity free inhibitor is manifested by its decreased backbone flexibility.

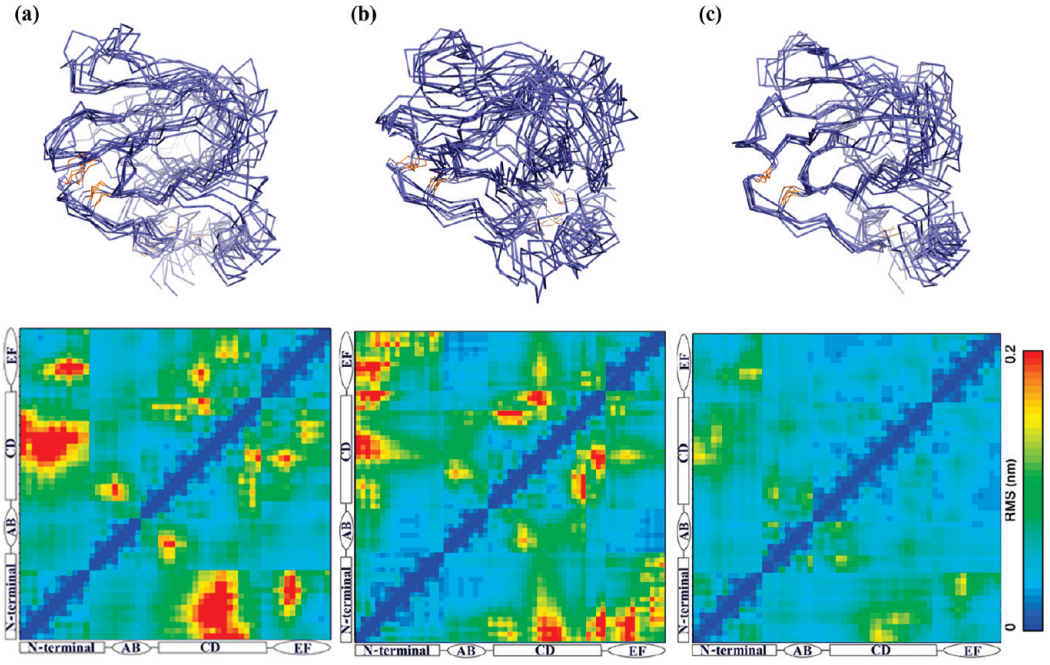


FIGURE 3: Influence of point mutations on the intrinsic dynamics of N-TIMP-1. Overlay of seven MD snapshots (sampled every 1 ns) of WT N-TIMP-1 (a), N-TIMP-1 T98A (b), and N-TIMP-1 T98L (c) in an orientation similar to that in Figure 1a. The introduction of the T98L mutation induces changes in the dynamic properties of N-TIMP-1, which are manifested by rigidification of the binding interface. The bottom panels show pairwise two-dimensional maps of internal distances describing the intrinsic flexibility of the TIMP binding interface residues in the unbound state of N-TIMP-1 WT (a), N-TIMP-1 T98A (b), and N-TIMP-1 T98L (c), demonstrating that WT N-TIMP-1 and the T98A mutant are more dynamic than the T98L mutant.

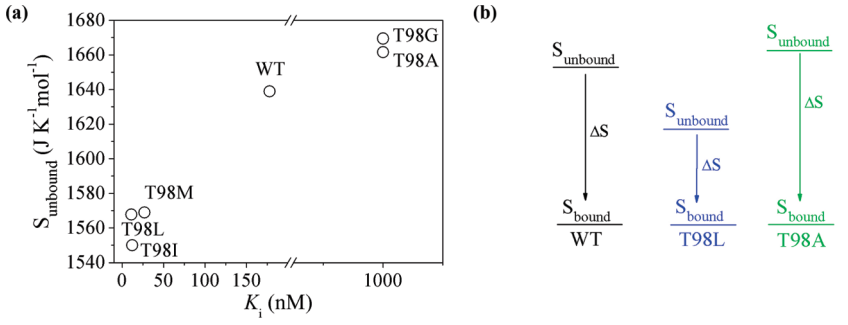


FIGURE 4: Correlation between inhibition capability and conformational entropy. (a) The correlation between inhibition constants ($K_i$) and the conformational entropy of the unbound state ($S_{unbound}$) shows that high-affinity mutants (T98L, T98I, and T98M) have reduced conformational entropy of the unbound protein compared with low-affinity mutants (WT, T98G, and T98A). (b) Schematic plot illustrating that the T98L mutation led to a reduced entropy cost ($\Delta S$) upon formation of the complex, making the binding thermodynamically more favorable.

TIMP variants, whose unbound states have a lower entropy and a more rigid binding interface, favor binding because the net change in entropy upon binding, $\Delta S$ ($S_{unbound} - S_{bound}$), is smaller than the $\Delta S$ of higher-entropy variants (Figure 4b). Thus, the entropy cost upon formation of the complex for high-affinity TIMP variants is smaller than for low-affinity TIMP variants. Hence, the T98L mutant forms a thermodynamically more stable complex with MT1-MMP by decreasing the binding entropy. This entropy effect is in agreement with reported titration calorimetry analysis of the MMP-3 and N-TIMP-1 complex quantifying the association of two well-structured proteins (*46*). Thus, the T98L mutation affected the driving force for enzyme−inhibitor association via protein backbone conformational dynamics.

Examination of the internal hydrogen bond network within the N-TIMP-1 interface among the different high- and low-affinity variants suggests that a single point mutation at Thr$^{98}$ affects the hydrogen bond stability at the inhibitor binding interface (Figure 5a). In general, five main chain hydrogen bonds are intimately involved in the conformational stability of TIMP's binding interface when bound to MMP (*18*, *21*). Our model indicates that a similar hydrogen bond network exists in the N-TIMP-1 binding interface [Cys$^1$−Ser$^{68}$, Val$^{69}$−Met$^{66}$, Gly$^{71}$−Met$^{66}$, Cys$^{70}$−Glu$^{67}$, and Cys$^{70}$−Thr$^{98}$ (Figure 5b)] when it is bound to MT1-MMP. This network of hydrogen bonds stabilizes the CD and EF loops that compose the binding interface. Importantly, the hydrogen bond between Cys$^1$ and Ser$^{68}$ may position the amino and carboxyl groups of Cys$^1$ to effectively coordinate the $Zn^{2+}$ ion. Thus, increased occupancy of these intramolecular hydrogen bonds in the unbound N-TIMP-1 interface contributes to the formation of a more structured and thus productive bound-like conformation. The hydrogen bond occupancy was defined as the percentage of simulation time during which a hydrogen bond N−O distance was less than 0.33 nm. This number was averaged over all independent MD runs. Statistical analysis of the key hydrogen bond stabilities in the N-TIMP-1

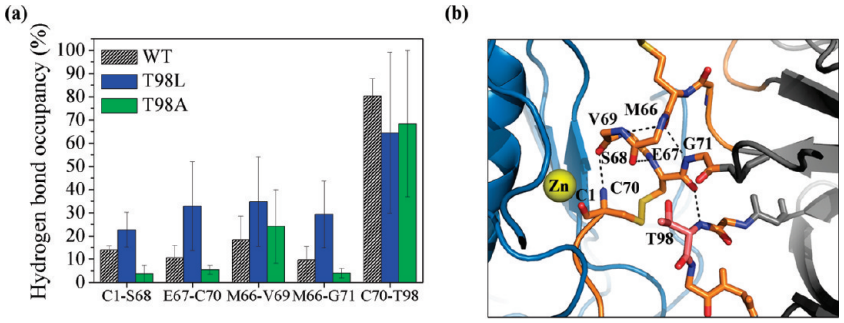


FIGURE 5: Network of intramolecular hydrogen bonds in N-TIMP-1 that stabilizes the complex. (a) Stability of key interfacial hydrogen bonds. The hydrogen bond stability was defined as the percentage of simulation time (along the 20 ns trajectory) during which a hydrogen bond N−O distance was less than 0.33 nm. This number was averaged over three or four independent MD runs. The T98L mutant possesses an increased stability of these hydrogen bonds. (b) N-TIMP-1 intramolecular hydrogen bond network (in orange sticks), when bound to MT1-MMP. This network involves residues from the N-terminal segment, the CD loop, and the EF loop. Dotted lines connect atoms involved in hydrogen bonds.

T98L mutant reveals that the hydrogen bonds between residues Cys[1] and Ser[68], Cys[70] and Glu[67], Gly[71] and Met[66], and Val[69] and Met[66] are significantly more stable than those in WT N-TIMP-1 (Figure 5a). The hydrogen bond between Cys[70] and Leu[98] does not seem to follow this trend, and its stability is reduced compared with that of WT N-TIMP-1. However, because of the large error associated with this measurement, we cannot conclude that this bond is becoming less stable upon mutation to leucine. In fact, in two trajectories, this bond is even more stable than the WT bond. Nevertheless, it is apparent that this hydrogen bond is significantly more stable in all N-TIMP-1 variants than the other intramolecular hydrogen bonds in all N-TIMP-1 variants, and therefore, the effect of a point mutation on it should have a smaller impact. Thus, mutations that enhance hydrogen bond stability contribute to the stability of the bound-like, less flexible, conformation of N-TIMP-1, which eventually results in increasing binding affinity for MT1-MMP.

Overall, our results indicate that WT N-TIMP-1 cannot form a tight-binding complex with MT1-MMP because of the intrinsic backbone flexibility of its binding interface. However, N-TIMP-1 forms tight-binding complexes with other members of the MMP family. This raises the question about the molecular determinants differentiating MT1-MMP from other members of the MMP family. Comparison of mean rmsd values per residue profiles among available NMR structures of various MMPs reveals remarkable differences in protein backbone dynamics (*47*) despite the high degree of identity in their sequence and structure. Because there is at present no available NMR structure of MT1-MMP, we performed 10 ns MD simulations on the unbound MT1-MMP, to gain insights into the dynamic properties of this enzyme. In comparison, we also performed MD simulations on the MMP-3 catalytic domain as a representative member of the MMP family that does form a tight-binding complex with WT N-TIMP-1. Panels a and b of Figure 6 depict the root-mean-square fluctuation (rmsf) per residue profiles of the catalytic domains of MMP-3 and MT1-MMP, respectively, aligned by sequence. Interestingly, the loop spanning residues 190−200 of MT1-MMP has a large rmsf value of ~0.6 nm, compared with the corresponding residues of MMP-3. This loop interacts with the AB and CD loops of N-TIMP-1, and therefore, its intrinsic dynamic properties may interfere with binding to the highly flexible TIMP-1 interface. Remarkably, the inhibitor T98L mutant exhibits a reduced flexibility (detected by lower rmsf values) of the distal AB loop residues 30−35 and the CD loop residues 65−70 compared with that of WT N-TIMP-1 (Figure 6c), which increases the probability for interaction with

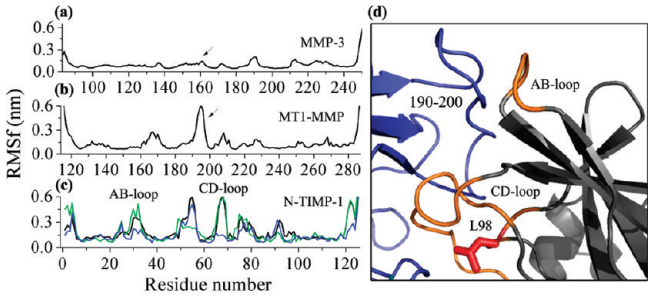


FIGURE 6: Enzyme loop dynamics regulates complex formation. (a and b) Root-mean-square fluctuation per residue profiles of the catalytic domains of MMP-3 as a representative member of the MMP family (a) and MT1-MMP (b) derived from 10 ns MD simulations. The sequences of both MMPs are aligned. (c) Root-mean-square fluctuation per residue profiles of WT N-TIMP-1 (black), N-TIMP-1 T98L (blue), and N-TIMP-1 T98A (green). A decrease in rmsd values of WT N-TIMP-1 with the T98L mutation was observed for the CD loop and for the distal AB loop, which is 16 Å from Thr[98]. MT1-MMP possesses a highly dynamic loop spanning residues 190−200, which may interfere with binding to the flexible AB and CD loops of N-TIMP-1 (d). This may explain the low affinity of MT1-MMP for N-TIMP-1 and how the change in inhibitor affinity changes the inhibitor function.

the dynamic loop of MT1-MMP. Noteworthy is the fact that the loop between residues 50 and 60 of N-TIMP-1 which is located opposite to the binding interface is also found to be as flexible as the CD loop, and mutation to leucine does not affect its dynamics. However, we cannot explain why mutation to alanine also results in a reduced flexibility of this loop. Thus, our data suggest that single point mutations in N-TIMP-1 at distal positions control overall backbone motion important for function. Thus, the effect of this mutation propagates away to other parts of the protein, indicating long-range communication within the protein core and the protein surface.

We have recently determined the high-resolution crystal structure of the complex formed between the catalytic domain of MT1-MMP and a representative high-affinity mutant of N-TIMP-1, V4A/P6V/T98L, at 2 Å resolution (Figure 7a, and see Table 1 of the Supporting Information for structure statistics). Alignment of the obtained crystal structure with the homology model of this N-TIMP-1 variant in a complex with MT1-MMP resulted in a low rmsd value of 1.2 Å (Figure S4 of the Supporting Information) which indicates the accuracy of our homology modeling analysis of the various MT1-MMP−N-TIMP-1 variant complexes used in the MD simulations. Two copies of the MT1-MMP−N-TIMP-1 V4A/P6V/T98L complex are located in the

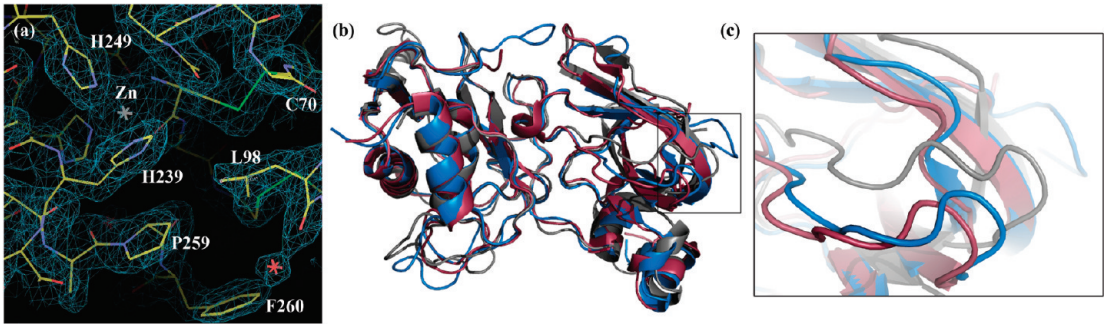


FIGURE 7: Structural insights into formation of the MT1-MMP−N-TIMP-1 complex. (a) Electron density map from the MT1-MMP−N-TIMP-1 crystal structure, centered around N-TIMP-1 $Leu^{98}$, which does not form any steric interference with MT1-MMP. $Leu^{98}$ is pointing toward MT1-MMP residues $Pro^{259}$ and $Phe^{260}$, establishing a strong hydrophobic core. Also, the catalytic zinc ion surrounded by $His^{239}$, $His^{243}$, and $His^{249}$ is shown. (b) Structural alignment of the crystal structure of the MT1-MMP−N-TIMP-1 complex (purple) with the crystal structures of the MMP-3−TIMP-1 complex (blue) and our MMP-1−N-TIMP-1 complex (gray). In the box are residues 73−83 of N-TIMP-1 that display high conformational variability (shown in larger scale in panel c) among all N-TIMP-1 complex crystal structures. Such differences are located throughout the entire N-TIMP-1 $\beta$-barrel. This figure was created using PyMol.

crystallographic asymmetric unit with a minor all-atom rmsd of 0.18 Å. The catalytic domain of MT1-MMP exhibits the typical MMP architecture and is similar to the previously determined structure of MT1-MMP in complex with TIMP-2 (rmsd of 0.53 Å) (*21*), except for a main difference in the conformation of the MT loop. Similarly, alignment with the crystal structure of MT3-MMP (*29*) also reveals differences only in the MT loop conformation, emphasizing its role as a special feature of MT-MMPs.

Comparative structural analysis with available crystal structures of MMP−TIMP complexes provides detailed insight into the molecular modes mediating effective physiological enzyme−inhibitor interactions. Superpositions of our crystal structure with the previously determined structures of MMP-3−TIMP-1 (*18*) and MMP-1−N-TIMP-1 (*48*) complexes (with respect to the MMP) reveal a similar binding conformation of the N-TIMP-1 interface with overall Cα rmsd values of 0.67 and 0.77 Å, respectively (Figure 7b). Noteworthy differences between the various crystal structures are detected at the N-TIMP-1 $\beta$-barrel (residues 50−60 and 73−83) (Figure 7c). NMR relaxation experiments showed that this $\beta$-barrel becomes more dynamic upon binding of MMP-3 to N-TIMP-1 (*46*). Thus, the different conformations detected by X-ray crystallography may reflect the flexibility of this area. Interestingly, we could not determine electron density for residues 50−57 of N-TIMP-1, which may further indicate on this loop intrinsic flexibility as suggested by our computational analysis (Figure 6c).

Comparative analyses of van der Waals (vdw) interactions at the binding interface and intermolecular hydrogen bonding interactions between our crystal structure and the previously determined MMP-TIMPs are presented in Tables 2 and 3 of the Supporting Information. These analyses indicate that each MMP forms different contacts and interactions with N-TIMP-1 despite their high degree of sequence and structural similarity. This may account for the differences in binding affinities and specificities of the inhibitors and their target enzymes. The protein−protein interactions formed between MT1-MMP and N-TIMP-1 are somewhat more similar in nature to the contacts formed between MMP-3 and N-TIMP-1, while MMP-1 adopts a significantly different binding interface as demonstrated previously (*48*). Interestingly, MT1-MMP forms five and nine fewer vdw interactions with N-TIMP-1 than MMP-3 and MMP-1, respectively, which may account in part for the lower affinity of N-TIMP-1 for MT1-MMP. In the crystal structure (Figure 7a), $Leu^{98}$ of mutated N-TIMP-1 forms a vdw contact with $Pro^{259}$ of MT1-MMP; however, it seems unlikely that this single additional bond could account for the entire binding effect between MT1-MMP and N-TIMP-1. Nevertheless, the reduced flexibility of the binding interface of N-TIMP-1 T98L may be rationalized from the crystal structure. $Thr^{98}$ in WT N-TIMP-1 is located near the disulfide bond formed between $Cys^{1}$ and $Cys^{70}$ and points toward two hydrophobic residues of MT1-MMP, $Pro^{259}$ and $Phe^{260}$. Sequence alignment of all known MMPs reveals that phenylalanine at this position is a unique motif of MT-MMPs. Replacement of $Thr^{98}$ with leucine may stabilize the entire area by establishing a strong hydrophobic core (Figure 7a) upon binding to the enzyme. This analysis complements the results obtained from MD simulation indicating that the point mutation in N-TIMP-1 reduced the conformational entropy of the free inhibitor, resulting in a significant decrease in backbone flexibility which led to effective binding and inhibition of MT1-MMP utilizing strong hydrophobic interactions.

Our results clearly demonstrate that a single point mutation affecting binding interface flexibility in N-TIMP-1 modifies the binding mechanism from poor binding to tight binding, as reflected by the increased association rate constant of the N-TIMP-1 T98L mutant. These results are consistent with a growing number of reports that link protein backbone flexibility to the molecular binding modes. By applying molecular simulations on four antibodies during different stages of maturation, it was shown that high-affinity antigen−antibody interactions are achieved by a loss of backbone flexibility of the unbound state of the antibody and a decrease in the entropic cost of binding (*49*). The apparent reduction in backbone flexibility of mature antibodies dominated "lock and key" binding mechanisms over "induced fit" mechanisms assigned for the premature more flexible antibodies. Such a binding mechanism may also describe N-TIMP-1 T98L binding to MT1-MMP, given the increased association constant of this mutant compared with that of WT N-TIMP-1. The coupling between protein affinity and flexibility was also demonstrated for transcription factors during binding to DNA (*50*). In this case, a direct link was found between an increase in the mobility and flexibility of the DNA recognition helix in transcription factor Elk-1 and its weaker affinity for DNA. This study further suggested that residues that are distal to the binding interface indirectly modulate the binding affinity by stabilizing the protein scaffold required for efficient DNA interactions. The impact of structural fluctuations on molecular recognition was also demonstrated on the C-terminal src homology 3 (SH3) domain of the

*Caenorhabditis elegans* protein SEM5 (SEM5 C-SH3) (*51*). These conserved domains mediate protein−protein interactions in signaling pathways by recognizing proline-rich sequences. Conformational fluctuations in SH3 domains, specifically in a loop adjacent to the binding site, were found to contribute significantly to the binding energetics observed for this regulatory protein domain. Importantly, mutations at this loop region were shown to affect binding through perturbations of conformational fluctuations and by changing the binding energetics by predictable and measurable way. Moreover, it was recently demonstrated that the rational design of allosteric point mutations in adenylate kinase can affect the conformational ensemble by increasing the population of the protein folded conformational state required for strong binding (*52*).

Our work further emphasizes the role of conformational entropy in mediating selective enzyme−inhibitor interactions. In N-TIMP-1, the reduction in the protein interface flexibility by a mutation in the binding interface periphery led to decreased conformational entropy influencing the thermodynamics of binding. Similarly, it was demonstrated that changes in the protein conformational entropy can contribute significantly to the free energy of protein−ligand interaction of the protein calmodulin with a variety of target domains (*53*). In addition, the apparent change in the corresponding conformational entropy could be related to the overall binding entropy indicating that these changes contribute significantly to the free energy of protein−ligand association. Interestingly, it was recently demonstrated that entropy-driven protein motions led to strong DNA−protein binding interactions suggesting that conformational entropy also plays a role in highly selective molecular recognition events (*54*).

Our work expands the scope of previous reports by highlighting the role of conformational selection and protein flexibility in mediating effective and/or selective inhibition of the important clinical target enzymes, MMPs, by their endogenous inhibitors, TIMPs. The general mechanism of TIMP inhibition of MMPs has been elucidated on the basis of the crystal structures of the TIMP−MMPs, yet the crystal structure of the MT1-MMP−N-TIMP-1 V4A/P6V/T98L complex (Figure 7) provides an only limited explanation of how this point mutation changed the function of TIMP-1. Molecular dynamics simulations of engineered N-TIMP-1 molecules showed that conformational dynamics is instrumental to productive complex formation with target MMPs. The association of MMPs with a variety of pathological states has stimulated impressive efforts over the past 20 years in the development of synthetic compounds capable of potently and selectively blocking the uncontrolled activity of these enzymes (*55*, *56*). Cuniasse et al. (*57*) have recently discussed the data on the inherent flexibility of the MMP active site and how this limits the utility of crystal structures and molecular modeling for the development of synthetic inhibitors. Moreover, Solomon et al. reported the effect of long-range protein conformational changes on active site chemical potential during catalysis by metalloproteinase (*58*). Disappointing results from clinical trials of such small molecule MMP inhibitors raise the notion that the only effective in vivo inhibitors identified to date are the TIMPs. Current efforts are invested in the engineering of TIMP molecules and their fragments toward more selective inhibitors targeting MMP in vivo activity (*31*, *59*, *60*). Our data suggest that directing protein conformational ensembles toward high-affinity binding conformers via site-directed mutagenesis at allosteric or remote sites may be used as a tool to advance the design of effective engineered TIMP fragments. Controlling intrinsic dynamics of engineered TIMPs or other endogenous MMP inhibitory domains, such as the pro domain, may also result in highly selective inhibitors targeted at individual MMPs.

## ACKNOWLEDGMENT

We thank Drs. Tzvia Selzer, Yoav Peleg, and Magdalini Rapti for their technical support. We also thank Dr. Igor Berezovsky for critically reading the manuscript.

## SUPPORTING INFORMATION AVAILABLE

Full MD trajectories, protein crystallography structural statistics, and structural analysis tables. This material is available free of charge via the Internet at http://pubs.acs.org.

## REFERENCES

1. Eisenmesser, E. Z., Millet, O., Labeikovsky, W., Korzhnev, D. M., Wolf-Watz, M., Bosco, D. A., Skalicky, J. J., Kay, L. E., and Kern, D. (2005) Intrinsic dynamics of an enzyme underlies catalysis. *Nature 438*, 117–121.
2. Boehr, D. D., McElheny, D., Dyson, H. J., and Wright, P. E. (2006) The dynamic energy landscape of dihydrofolate reductase catalysis. *Science 313*, 1638–1642.
3. Miyashita, O., Onuchic, J. N., and Wolynes, P. G. (2003) Nonlinear elasticity, proteinquakes, and the energy landscapes of functional transitions in proteins. *Proc. Natl. Acad. Sci. U.S.A. 100*, 12570–12575.
4. Smock, R. G., and Gierasch, L. M. (2009) Sending signals dynamically. *Science 324*, 198–203.
5. Ikeguchi, M., Ueno, J., Sato, M., and Kidera, A. (2005) Protein structural change upon ligand binding: Linear response theory. *Phys. Rev. Lett. 94*, 078102.
6. Teague, S. J. (2003) Implications of protein flexibility for drug discovery. *Nat. Rev. Drug Discovery 2*, 527–541.
7. Tokuriki, N., and Tawfik, D. S. (2009) Protein dynamism and evolvability. *Science 324*, 203–207.
8. Watney, J. B., Agarwal, P. K., and Hammes-Schiffer, S. (2003) Effect of mutation on enzyme motion in dihydrofolate reductase. *J. Am. Chem. Soc. 125*, 3745–3750.
9. Maillard, R. A., Jordan, M., Beasley, D. W., Barrett, A. D., and Lee, J. C. (2008) Long range communication in the envelope protein domain III and its effect on the resistance of West Nile virus to antibody-mediated neutralization. *J. Biol. Chem. 283*, 613–622.
10. Clarkson, M. W., and Lee, A. L. (2004) Long-range dynamic effects of point mutations propagate through side chains in the serine protease inhibitor eglin c. *Biochemistry 43*, 12448–12458.
11. Pizzitutti, F., Giansanti, A., Ballario, P., Ornaghi, P., Torreri, P., Ciccotti, G., and Filetici, P. (2006) The role of loop ZA and Pro371 in the function of yeast Gcn5p bromodomain revealed through molecular dynamics and experiment. *J. Mol. Recognit. 19*, 1–9.
12. Pan, H., Lee, J. C., and Hilser, V. J. (2000) Binding sites in *Escherichia coli* dihydrofolate reductase communicate by modulating the conformational ensemble. *Proc. Natl. Acad. Sci. U.S.A. 97*, 12020–12025.
13. Nagase, H., and Woessner, J. F., Jr. (1999) Matrix metalloproteinases. *J. Biol. Chem. 274*, 21491–21494.
14. Sternlicht, M. D., and Werb, Z. (2001) How matrix metalloproteinases regulate cell behavior. *Annu. Rev. Cell. Dev Biol. 17*, 463–516.
15. Lopez-Otin, C., and Matrisian, L. M. (2007) Emerging roles of proteases in tumour suppression. *Nat. Rev. Cancer 7*, 800–808.
16. Page-McCaw, A., Ewald, A. J., and Werb, Z. (2007) Matrix metalloproteinases and the regulation of tissue remodelling. *Nat. Rev. Mol. Cell Biol. 8*, 221–233.
17. Birkedal-Hansen, H. (1995) Proteolytic remodeling of extracellular matrix. *Curr. Opin. Cell Biol. 7*, 728–735.
18. Gomis-Ruth, F. X., Maskos, K., Betz, M., Bergner, A., Huber, R., Suzuki, K., Yoshida, N., Nagase, H., Brew, K., Bourenkov, G. P., Bartunik, H., and Bode, W. (1997) Mechanism of inhibition of the human matrix metalloproteinase stromelysin-1 by TIMP-1. *Nature 389*, 77–81.
19. Tuuttila, A., Morgunova, E., Bergmann, U., Lindqvist, Y., Maskos, K., Fernandez-Catalan, C., Bode, W., Tryggvason, K., and Schneider, G. (1998) Three-dimensional structure of human tissue inhibitor of metalloproteinases-2 at 2.1 Å resolution. *J. Mol. Biol. 284*, 1133–1140.

20. Williamson, R. A., Martorell, G., Carr, M. D., Murphy, G., Docherty, A. J., Freedman, R. B., and Feeney, J. (1994) Solution structure of the active domain of tissue inhibitor of metalloproteinases-2. A new member of the OB fold protein family. *Biochemistry 33*, 11745–11759.
21. Fernandez-Catalan, C., Bode, W., Huber, R., Turk, D., Calvete, J. J., Lichte, A., Tschesche, H., and Maskos, K. (1998) Crystal structure of the complex formed by the membrane type 1-matrix metalloproteinase with the tissue inhibitor of metalloproteinases-2, the soluble progelatinase A receptor. *EMBO J. 17*, 5238–5248.
22. Maskos, K., Lang, R., Tschesche, H., and Bode, W. (2007) Flexibility and variability of TIMP binding: X-ray structure of the complex between collagenase-3/MMP-13 and TIMP-2. *J. Mol. Biol. 366*, 1222–1231.
23. Huang, W., Suzuki, K., Nagase, H., Arumugam, S., Van Doren, S. R., and Brew, K. (1996) Folding and characterization of the amino-terminal domain of human tissue inhibitor of metalloproteinases-1 (TIMP-1) expressed at high yield in *E. coli*. *FEBS Lett. 384*, 155–161.
24. Murphy, G., Houbrechts, A., Cockett, M. I., Williamson, R. A., O'Shea, M., and Docherty, A. J. (1991) The N-terminal domain of tissue inhibitor of metalloproteinases retains metalloproteinase inhibitory activity. *Biochemistry 30*, 8097–8102.
25. Nguyen, Q., Willenbrock, F., Cockett, M. I., O'Shea, M., Docherty, A. J., and Murphy, G. (1994) Different domain interactions are involved in the binding of tissue inhibitors of metalloproteinases to stromelysin-1 and gelatinase A. *Biochemistry 33*, 2089–2095.
26. Lee, M. H., Knauper, V., Becherer, J. D., and Murphy, G. (2001) Full-length and N-TIMP-3 display equal inhibitory activities toward TNF-α convertase. *Biochem. Biophys. Res. Commun. 280*, 945–950.
27. Sato, H., Kinoshita, T., Takino, T., Nakayama, K., and Seiki, M. (1996) Activation of a recombinant membrane type 1-matrix metalloproteinase (MT1-MMP) by furin and its interaction with tissue inhibitor of metalloproteinases (TIMP)-2. *FEBS Lett. 393*, 101–104.
28. Will, H., Atkinson, S. J., Butler, G. S., Smith, B., and Murphy, G. (1996) The soluble catalytic domain of membrane type 1 matrix metalloproteinase cleaves the propeptide of progelatinase A and initiates autoproteolytic activation. Regulation by TIMP-2 and TIMP-3. *J. Biol. Chem. 271*, 17119–17123.
29. Lang, R., Braun, M., Sounni, N. E., Noel, A., Frankenne, F., Foidart, J. M., Bode, W., and Maskos, K. (2004) Crystal structure of the catalytic domain of MMP-16/MT3-MMP: Characterization of MT-MMP specific features. *J. Mol. Biol. 336*, 213–225.
30. Lee, M. H., Rapti, M., Knauper, V., and Murphy, G. (2004) Threonine 98, the pivotal residue of tissue inhibitor of metalloproteinases (TIMP)-1 in metalloproteinase recognition. *J. Biol. Chem. 279*, 17562–17569.
31. Lee, M. H., Maskos, K., Knauper, V., Dodds, P., and Murphy, G. (2002) Mapping and characterization of the functional epitopes of tissue inhibitor of metalloproteinases (TIMP)-3 using TIMP-1 as the scaffold: A new frontier in TIMP engineering. *Protein Sci. 11*, 2493–2503.
32. Dudek, M. J., Ramnarayan, K., and Ponder, J. W. (1998) Protein structure prediction using a combination of sequence homology and global energy minimization: II. Energy functions. *J. Comput. Chem. 19*, 548–573.
33. Pettersen, E. F., Goddard, T. D., Huang, C. C., Couch, G. S., Greenblatt, D. M., Meng, E. C., and Ferrin, T. E. (2004) UCSF Chimera: A visualization system for exploratory research and analysis. *J. Comput. Chem. 25*, 1605–1612.
34. Van Gunsteren, W. F., Daura, X., and Mark, A. (1998) GROMOS force field. In Encyclopedia of Computational Chemistry, Vol. *2*, John Wiley & Sons, New York.
35. Scott, W. R. P., Hünenberger, P. H., Tironi, I. G., Mark, A. E., Billeter, S. R., Fennen, J., Torda, A. E., Huber, T., Krüger, P., and Van Gunsteren, W. F. (1999) The GROMOS Biomolecular Simulation Program Package. *J. Phys. Chem. A 103*, 3596–3607.
36. Berendsen, H. J. C., Postma, J. P. M., Van Gunsteren, W. F., DiNola, A., and Haak, J. R. (1984) Molecular dynamics with coupling to an external bath. *J. Chem. Phys. 81*, 3684.
37. Schlitter, J. (1993) Estimation of Absolute and Relative Entropies of Macromolecules Using the Covariance-Matrix. *Chem. Phys. Lett. 215*, 617–621.
38. Otwinowski, Z., and Minor, W. (1997) Processing of X-ray diffraction data collected in oscillation mode. *Methods Enzymol. 276*, 307–326.
39. French, G. S., and Wilson, K. S. (1978) On the treatment of negative intensity observations. *Acta Crystallogr. A34*, 517–525.
40. Murshudov, G. N., Vagin, A. A., and Dodson, E. J. (1997) Refinement of macromolecular structures by the maximum-likelihood method. *Acta Crystallogr. D53*, 240–255.
41. Emsley, P., and Cowtan, K. (2004) Coot: Model-building tools for molecular graphics. *Acta Crystallogr. D60*, 2126–2132.
42. Chen, V. B., Arendall, W. B., III, Headd, J. J., Keedy, D. A., Immormino, R. M., Kapral, G. J., Murray, L. W., Richardson, J. S., and Richardson, D. C. (2010) MolProbity: All-atom structure validation for macromolecular crystallography. *Acta Crystallogr. D66*, 12–21.
43. Rajamani, D., Thiel, S., Vajda, S., and Camacho, C. J. (2004) Anchor residues in protein-protein interactions. *Proc. Natl. Acad. Sci. U.S.A. 101*, 11287–11292.
44. Lee, M. H., Rapti, M., and Murphy, G. (2003) Unveiling the surface epitopes that render tissue inhibitor of metalloproteinase-1 inactive against membrane type 1-matrix metalloproteinase. *J. Biol. Chem. 278*, 40224–40230.
45. Grunberg, R., Nilges, M., and Leckner, J. (2006) Flexibility and conformational entropy in protein-protein binding. *Structure 14*, 683–693.
46. Arumugam, S., Gao, G., Patton, B. L., Semenchenko, V., Brew, K., and Van Doren, S. R. (2003) Increased backbone mobility in β-barrel enhances entropy gain driving binding of N-TIMP-1 to MMP-3. *J. Mol. Biol. 327*, 719–734.
47. Bertini, I., Calderone, V., Cosenza, M., Fragai, M., Lee, Y. M., Luchinat, C., Mangani, S., Terni, B., and Turano, P. (2005) Conformational variability of matrix metalloproteinases: Beyond a single 3D structure. *Proc. Natl. Acad. Sci. U.S.A. 102*, 5334–5339.
48. Iyer, S., Wei, S., Brew, K., and Acharya, K. R. (2007) Crystal structure of the catalytic domain of matrix metalloproteinase-1 in complex with the inhibitory domain of tissue inhibitor of metalloproteinase-1. *J. Biol. Chem. 282*, 364–371.
49. Thorpe, I. F., and Brooks, C. L., III (2007) Molecular evolution of affinity and flexibility in the immune system. *Proc. Natl. Acad. Sci. U.S.A. 104*, 8821–8826.
50. Park, S., Boder, E. T., and Saven, J. G. (2005) Modulating the DNA affinity of Elk-1 with computationally selected mutations. *J. Mol. Biol. 348*, 75–83.
51. Manson, A., Whitten, S. T., Ferreon, J. C., Fox, R. O., and Hilser, V. J. (2009) Characterizing the role of ensemble modulation in mutation-induced changes in binding affinity. *J. Am. Chem. Soc. 131*, 6785–6793.
52. Schrank, T. P., Bolen, D. W., and Hilser, V. J. (2009) Rational modulation of conformational fluctuations in adenylate kinase reveals a local unfolding mechanism for allostery and functional adaptation in proteins. *Proc. Natl. Acad. Sci. U.S.A. 106*, 16984–16989.
53. Frederick, K. K., Marlow, M. S., Valentine, K. G., and Wand, A. J. (2007) Conformational entropy in molecular recognition by proteins. *Nature 448*, 325–329.
54. Tzeng, S. R., and Kalodimos, C. G. (2009) Dynamic activation of an allosteric regulatory protein. *Nature 462*, 368–372.
55. Whittaker, M., Floyd, C. D., Brown, P., and Gearing, A. J. (1999) Design and therapeutic application of matrix metalloproteinase inhibitors. *Chem. Rev. 99*, 2735–2776.
56. Cuniasse, P., Devel, L., Makaritis, A., Beau, F., Georgiadis, D., Matziari, A., Yiotakis, A., and Dive, V. (2005) Future challenges facing the development of specific active-site-directed synthetic inhibitors of MMPs. *Biochimie 87*, 393–402.
57. Cuniasse, P., Devel, L., Makaritis, A., Beau, F., Georgiadis, D., Matziari, M., Yiotakis, A., and Dive, V. (2005) Future challenges facing the development of specific active-site-directed synthetic inhibitors of MMPs. *Biochimie 87*, 393–402.
58. Solomon, A., Akabayov, B., Frenkel, A., Milla, M. E., and Sagi, I. (2007) Key feature of the catalytic cycle of TNF-α converting enzyme involves communication between distal protein sites and the enzyme catalytic core. *Proc. Natl. Acad. Sci. U.S.A. 104*, 4931–4936.
59. Meng, Q., Malinovskii, V., Huang, W., Hu, Y., Chung, L., Nagase, H., Bode, W., Maskos, K., and Brew, K. (1999) Residue 2 of TIMP-1 is a major determinant of affinity and specificity for matrix metalloproteinases but effects of substitutions do not correlate with those of the corresponding P1′ residue of substrate. *J. Biol. Chem. 274*, 10184–10189.
60. Hamze, A. B., Wei, S., Bahudhanapati, H., Kota, S., Acharya, K. R., and Brew, K. (2007) Constraining specificity in the N-domain of tissue inhibitor of metalloproteinases-1: Gelatinase-selective inhibitors. *Protein Sci. 16*, 1905–1913.